

Particle Size Effects on Chemistry and Structure of Al-Cu-Fe Quasicrystalline Coatings

D.J. Sordelet, M.F. Besser, and I.E. Anderson

Gas atomized $\text{Al}_{63}\text{Cu}_{25}\text{Fe}_{12}$ powders of varying size fractions were plasma sprayed onto hot (~600 °C) and cool (~25 °C) substrates using Mach I and subsonic plasma gun configurations. The chemical composition and phase contents of coatings were determined. Furthermore, coatings were annealed in vacuum at 700 °C for 2 h to observe phase changes. It was found that finer particles (e.g., <25 μm) tend to vaporize Al during spraying, which shifts the coating composition away from the quasicrystalline (ψ) single-phase region in the Al-Cu-Fe phase diagram. Coatings deposited on hot substrates were denser, richer in the ψ phase, and harder than the corresponding coatings deposited onto cool substrates.

1. Introduction

QUASICRYSTALS are well-ordered, but aperiodic, structures with classically forbidden rotation symmetries (e.g., icosahedral or decagonal) (Ref 1). Since the unexpected discovery of quasicrystalline structures in 1984 (Ref 2), research studies have focused mostly on understanding atomic structure (Ref 3) and phase equilibrium (Ref 4, 5). More recently, scientists have begun to recognize the potential usefulness of quasicrystals in engineering applications (Ref 6, 7). For example, the hardness and stiffness characteristics of quasicrystals formed from the Al-Cu-Fe system suggest that the materials should exhibit low-friction, wear-resistant behavior (Ref 8). Indeed, a number of studies have supported this hypothesis (Ref 9, 10). Other research has shown that some Al-based quasicrystals are resistant to excessive oxidation (Ref 11-13).

To date, hundreds of metal alloys have been identified to display a quasicrystalline phase (Ref 14). Many quasicrystalline systems require rapid solidification methods, such as melt spinning, in order to form. Tsai et al. (Ref 15) found that the Al-Cu-Fe system forms a quasicrystalline phase that is stable at temperatures very close to its melting point. This discovery precipitated numerous efforts to characterize the mechanical properties of Al-Cu-Fe quasicrystals (Ref 16, 17). A portion of the research within the authors' laboratory is aimed at evaluating plasma-sprayed (PS) quasicrystal coatings for automotive and agricultural applications. In addition, the attractive economical and environmental features of Al-Cu-Fe alloys have motivated studies to evaluate quasicrystal coatings as replacements for electrodeposited chromium coatings.

One feature of the Al-Cu-Fe system, which has hindered the synthesis of macroscopic, single-phase, single-grain quasicrystals, is its complex solidification behavior. Early work with this system (Ref 18, 19) identified a complex phase centered approximately around $\text{Al}_{63}\text{Cu}_{25}\text{Fe}_{12}$. The authors were unable to define this phase, which they termed as ψ , using x-ray diffraction (XRD). It is now known that the ψ phase has a quasicrystalline structure. More recent surveys of the Al-Cu-Fe system

were performed to better understand the phase relationships between the ψ phase and its neighboring crystalline phases (Ref 5). Note that a composition of $\text{Al}_{63}\text{Cu}_{25}\text{Fe}_{12}$ was used throughout the current study. This composition falls within the single-phase ψ region of the Al-Cu-Fe phase diagram. The ψ phase has equilibrium relationships with a cubic (β) phase and a monoclinic (λ) phase. Typical compositions of the β and λ phases that formed during processing (e.g., chill casting) are $\text{Al}_{55}\text{Cu}_{40}\text{Fe}_5$ and $\text{Al}_{72}\text{Cu}_5\text{Fe}_{23}$, respectively. These phases were described in more detail elsewhere (Ref 20).

Starting powders strongly affect the microstructure and properties of PS coatings (Ref 21). Consideration of starting powders is especially critical when forming Al-Cu-Fe quasicrystal PS coatings due to the complex solidification path of the alloy. Recent studies by the authors demonstrated that gas atomized $\text{Al}_{63}\text{Cu}_{25}\text{Fe}_{12}$ powders produced coatings that were much more homogeneous in chemical composition and phase structure than coatings prepared from powders obtained by crushing a cast ingot (Ref 20). These differences were the result of the contrasting solidification rates between the gas atomization and ingot casting processes; the former process yields much more homogeneous powders.

Whereas it is important to have homogeneous starting powders if a uniform coating microstructure is desired, it is equally necessary to have coating parameters that do not alter the composition of the powder. For example, metal carbides can easily decompose and oxidize during PS and form undesirable phases (Ref 22, 23). Similar difficulties can be encountered with alloy powders if selective vaporization of a particular element occurs. Material loss due to vaporization was reported to occur during air plasma spraying of ceramic superconductors (Ref 24). Quite likely, the problem of material loss is more widespread throughout the PS industry than is currently realized due to the lack of appropriate analytical capabilities in many coating facilities.

In the development of Al-Cu-Fe PS coatings, it is generally desired to maximize the fraction of the quasicrystal (ψ) phase. Furthermore, coatings intended for tribological applications typically require minimal porosity. Initial studies in our laboratory revealed that when using gas atomized $\text{Al}_{63}\text{Cu}_{25}\text{Fe}_{12}$ powder, finer starting powders produced higher densities, while coarser particles produced more of the ψ phase. These general observations were made while keeping all other processing parameters constant. The objective of the current study is to under-

Keywords Al-Cu-Fe coatings, coating chemistry, coating microstructure, particle size effects, quasicrystal

D.J. Sordelet, M.F. Besser, and I.E. Anderson, Ames Laboratory, U.S. DOE, Iowa State University, Ames, IA 50011, USA.

stand the role of starting powder particle size on PS coating chemistry, phase equilibrium, and grain structure.

2. Experimental Procedure

2.1 Starting Powders

Starting powders with a nominal composition of Al₆₃Cu₂₅Fe₁₂ were prepared by gas atomization using argon. Powders were screened or air classified into different particle size distributions for subsequent PS. The specific size fractions prepared were -25 µm; +25, -45 µm; +53, -63 µm; +45, -75 µm; and +75, -106 µm.

The as-atomized powder is primarily a two-phase mixture of the ψ and β phases. Therefore, portions of the five different powder sizes were annealed under vacuum at 700 °C for 14 h to form nearly single-phase ψ structures.

2.2 Plasma Spraying

The as-atomized and vacuum annealed starting powders were processed by PS using subsonic and Mach I plasma gun configurations. The gun components and operating parameters are listed in Table 1. The conditions shown in Table 1 were not selected to obtain a specific set of plasma temperatures or particle velocities. Rather, they were chosen to establish a reasonable

variation in power input and gas velocity so that differences in particle heating and in-flight reactivity could be observed.

The effect of substrate temperature was also studied during plasma spraying of the different powder sizes. Copper substrates were heated in a furnace until they reached approximately 650 °C. The substrates were removed, and spraying was initiated within a few seconds. Mild steel substrates were fixtured next to the Cu coupons during spraying. The steel substrates were air cooled from behind during coating. Also a thin

Table 1 Plasma gun configurations and spraying parameters

Parameter	Mode	
	Mach I	Subsonic
Plasma gun	SG-100(a)	SG-100(a)
Anode, part number	358	730
Cathode, part number	112	120
Gas injector, part number	113	112
Amps	800	700
Volts, @ gun	43.1	25.7
Arc gas, slpm	37.8 (Ar)	37.8 (Ar)
Auxiliary gas, slpm	20.0 (He)	0
Carrier gas, slpm	5.6 (Ar)	5.6 (Ar)
Powder feed rate, g/min	20.0	20.0
Stand off, cm	7.5	7.5

(a) Miller Thermal, Inc., Appleton, WI
Slpm is standard liters per minute.

Table 2 Coating sample descriptions

Coating label	Starting powder size, µm	Powder condition	Gun configuration	Substrate condition
1MH	-25	As-atomized	Mach I	Hot
2MH	+25, -45	As-atomized	Mach I	Hot
3MH	+53, -63	As-atomized	Mach I	Hot
4MH	+45, -75	As-atomized	Mach I	Hot
5MH	+75, -106	As-atomized	Mach I	Hot
1MC	-25	As-atomized	Mach I	Cool
2MC	+25, -45	As-atomized	Mach I	Cool
3MC	+53, -63	As-atomized	Mach I	Cool
4MC	+45, -75	As-atomized	Mach I	Cool
5MC	+75, -106	As-atomized	Mach I	Cool
1SH	-25	As-atomized	Subsonic	Hot
2SH	+25, -45	As-atomized	Subsonic	Hot
3SH	+53, -63	As-atomized	Subsonic	Hot
4SH	+45, -75	As-atomized	Subsonic	Hot
5SH	+75, -106	As-atomized	Subsonic	Hot
1SC	-25	As-atomized	Subsonic	Cool
2SC	+25, -45	As-atomized	Subsonic	Cool
3SC	+53, -63	As-atomized	Subsonic	Cool
4SC	+45, -75	As-atomized	Subsonic	Cool
5SC	+75, -106	As-atomized	Subsonic	Cool
1*MH	-25	Annealed	Mach I	Hot
4*MH	+45, -75	Annealed	Mach I	Hot
5*MH	+75, -106	Annealed	Mach I	Hot
1*MC	-25	Annealed	Mach I	Cool
4*MC	+45, -75	Annealed	Mach I	Cool
5*MC	+75, -106	Annealed	Mach I	Cool
1*SH	-25	Annealed	Subsonic	Hot
4*SH	+45, -75	Annealed	Subsonic	Hot
5*SH	+75, -106	Annealed	Subsonic	Hot
1*SC	-25	Annealed	Subsonic	Cool
4*SC	+45, -75	Annealed	Subsonic	Cool
5*SC	+75, -106	Annealed	Subsonic	Cool

(~0.1 cm) strip of mild steel, which was likewise air cooled from behind, was coated along with the Cu and steel substrates. The material deposited onto the thin strip of steel was removed for subsequent characterization.

The approximate temperatures of the Cu and steel substrate surfaces were continuously monitored by placing a type-K thermocouple into a hole drilled into the back of substrates. The tip of the thermocouple was 0.1 cm away from the surface being coated. Figure 1 shows a typical temperature profile of hot Cu and cool steel substrates during coating. Very similar temperature behavior was seen during all coating experiments.

A small piece of each coated steel substrate was heated in vacuum at 700 °C for 2 h to study the microstructural evolution of the as-sprayed material.

Coating samples discussed here are labeled as given in Table 2 according to starting powder size (1, 2, 3, 4, or 5), PS gun configuration (M or S), and substrate temperature (H or C). The powder size labels 1, 2, 3, 4, and 5 correspond, respectively, to the -25 µm; +25, -45 µm; +53, -63 µm; +45, -75 µm, and +75, -106 µm size fractions. The coatings prepared with starting powders that were vacuum annealed are identified with an asterisk (*) following the powder size label. The PS gun configuration labels M and S refer to Mach I and subsonic, respectively. The coatings deposited onto hot Cu substrates are labeled H, while those deposited onto cool steel substrates are labeled C. For example, the coating sprayed with -25 µm powder onto a hot Cu substrate using the Mach I gun assembly is described as 1MH. Table 2 provides a complete description of the coatings prepared in this study and their corresponding sample codes.

2.3 Characterization

The techniques described here were used to characterize starting powders and PS coatings. As-sprayed, i.e., bulk, coatings and powdered coatings (after removal from their substrate) were studied.

Inductively coupled plasma-atomic emission spectroscopy (ICP-AES) was used to determine Al, Cu, and Fe contents of starting powders and powdered coatings. Oxygen contents of the powders and coatings were measured using the inert gas fusion (IGF) technique on a Leco 12 system (LECO Corporation, St. Joseph, MD). The coating samples for the above chemical analyses were obtained by removing them from the thin steel strips described earlier.

XRD was used to determine the structures of starting powders, as-sprayed coatings, and powdered coatings. Powdered coating samples were obtained from material deposited onto hot Cu substrates and thin steel strips. XRD was performed with a Philips 1810 diffractometer (Philips Electronics North America, New York, NY) using CuK α radiation. Due to the large number of coating samples generated in the current study, most scans were performed between 42° and 46° 2θ. The primary peaks from the ψ and β phases fall within this range when using a CuK α source.

It is difficult to quantify the amounts of the ψ , β , and λ phases using XRD data. Conventional quantitative methods using structure factors are not straightforward due to the unknown atomic positions of the quasicrystalline ψ phase. An effort to ob-

tain some quantitative information was made by blending known amounts of single-phase ψ and β phase powders together. These powders were obtained from vacuum annealed cast ingots with compositions determined from previous re-

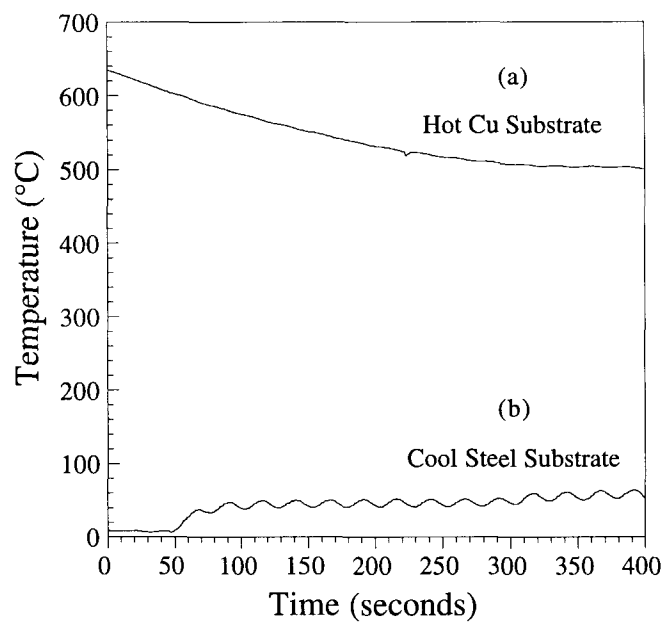


Fig. 1 Typical temperature profile of (a) Cu substrate and (b) steel substrate during plasma spraying

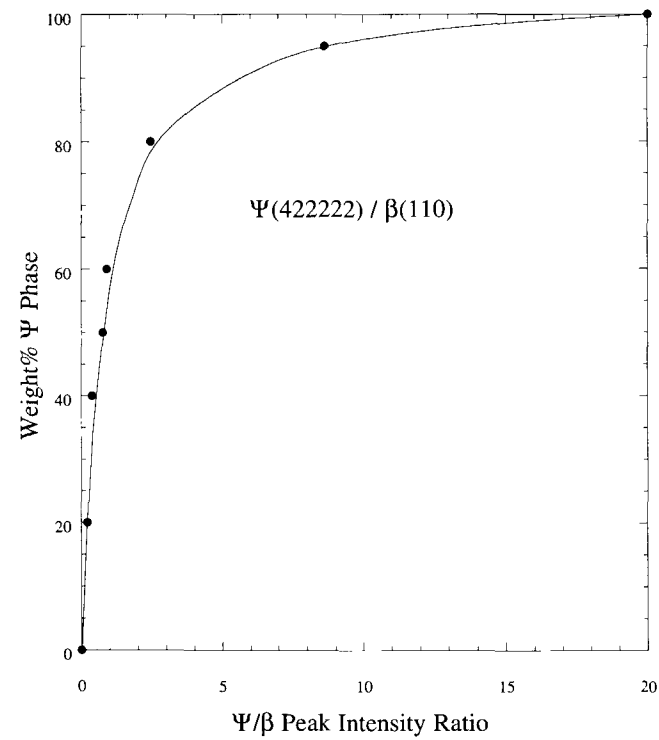


Fig. 2 Weight percent of ψ phase in a binary mixture of ψ and β powders as determined by peak intensity ratios of (42222) and (110) planes for ψ and β phases, respectively. See Ref 25 for an explanation of 6-digit indices used to identify the icosahedral (ψ) phase.

search (Ref 20). The XRD patterns obtained from the blended mixtures were analyzed by comparing specific peak intensities. Figure 2 displays the peak height ratios from the ψ and β phases as a function of ψ content. The data presented in Fig. 2 were obtained by comparing the (422222) and (110) peak intensities from the ψ and β phases, respectively. The six independent Miller indices used to identify the icosahedral phase are discussed in Ref 25. Very similar results were obtained by comparing the (420024) and (101000) ψ peaks to the (110) and (211) β peaks, respectively. The 2 θ locations of these specific peaks are identified in Fig. 3(a). These results provide a semiquantitative determination of phase contents in as-sprayed coatings discussed later. The curve in Fig. 2 was also used to estimate relative phase fractions in the as-atomized starting powders (Table 3).

Differential thermal analysis (DTA) was performed to compare the thermal events during heating of starting powders and powdered coatings. The DTA results were obtained with a Per-

kin Elmer System 7 unit (Perkin-Elmer Physical Electronics, Eden Prairie, MN). Scans were performed in flowing argon at a heating rate of 10 °C/min. Approximately 50 mg of powdered coating was analyzed in each run.

Coatings deposited onto hot Cu and cool steel substrates were prepared for metallographic examination. Epoxy mounts were prepared by vacuum impregnation of the coating. Grinding and polishing was performed on an automatic system using an initial 180-grit SiC paper followed by 9 and 3 μm lapping. A final polish with 0.05 μm Al_2O_3 was used to remove remaining scratches. Polished cross sections were observed using scanning electron microscopy (SEM) on a JOEL 6100 (JOEL, Peabody, MA) instrument.

Indentation hardness measurements were taken from polished coatings. Samples of several coatings deposited onto hot Cu and cool steel substrates were tested with a Vickers indenter using a 30 g load. Hardness values reported represent an average of five measurements.

Table 3 Chemical compositions of gas atomized starting powders

Powder size, μm	Al	Cu	Fe	O	ψ (a)
-25	42.4	39.7	16.4	0.205	69
+25, -45	42.3	39.7	16.9	0.112	63
+53, -63	42.1	39.8	16.9	0.083	60
+45, -75	42.0	39.9	16.7	0.080	60
+75, -106	42.0	40.5	16.4	0.065	55

Note: Composition of $\text{Al}_{63}\text{Cu}_{25}\text{Fe}_{12}$ is approximately 42.3 wt% Al, 40.0 wt% Cu, and 17.7 wt% Fe (a) ψ phase is based on calibration curve in Fig. 2

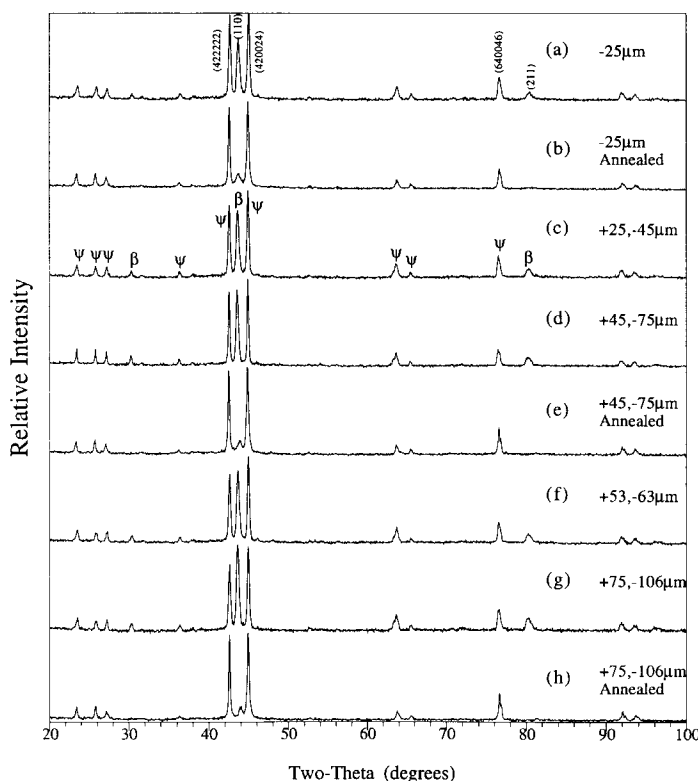


Fig. 3 XRD patterns of as-atomized and annealed starting powders. Powder size fractions are as follows: (a) -25 μm , (b) -25 μm annealed; (c) +25, -45 μm ; (d) +45, -75 μm ; (e) +45, -75 μm annealed; (f) +53, -63 μm ; (g) +75, -106 μm ; and (h) +75, -106 μm annealed. See Ref 25 for an explanation of 6-digit indices (Fig. 3a) used to identify the icosahedral (ψ) phase

3. Results

3.1 Composition and Structure of Starting Powders

Chemical compositions of the five starting powder size fractions determined by ICP-AES are displayed in Table 3. All powders are similar in Al, Cu, and Fe contents and are close to the targeted starting composition of $\text{Al}_{63}\text{Cu}_{25}\text{Fe}_{12}$. The bulk oxygen content clearly decreased with increasing average particle size. This strongly suggests that oxygen is present as a surface layer rather than a uniform bulk constituent.

Figure 3 shows the structures of the as-atomized powders. Also shown are XRD patterns obtained from the starting powders after vacuum annealing at 700 °C for 12 h. The as-atomized powders contain the quasicrystalline (ψ) and cubic (β) phases. As mentioned, the $\text{Al}_{63}\text{Cu}_{25}\text{Fe}_{12}$ composition also has equilibrium relationships with a monoclinic (λ) phase. However, its presence in the powder samples is difficult to determine by XRD because of the large number of scattering planes present in the low-symmetry monoclinic structure. Vacuum annealing produced a mostly single-phase ψ structure in all powder sizes; however, some of the cubic β phase remained.

Consistency of phases between powder sizes can be seen further by comparing DTA patterns. Figure 4 shows the melting behavior of the $-25\text{ }\mu\text{m}$ and $+75\text{, }-106\text{ }\mu\text{m}$ size fractions. The endothermic peak just below 900 °C represents the decomposition of ψ into liquid and $\beta + \lambda$. The higher temperature peaks correspond to final melting. The coarser powder (Fig. 4b) shows an additional endothermic reaction between 600 and 700 °C. This is likely melting of an Al_2Cu -type phase, which is often

seen with $\text{Al}_{63}\text{Cu}_{25}\text{Fe}_{12}$ composition under slower solidification conditions (e.g., ingot casting) (Ref 26).

Powder morphology and internal structure of the different powder size fractions are presented in Fig. 5. The $-25\text{ }\mu\text{m}$ powder has a large population of particles that are below $10\text{ }\mu\text{m}$. It is not clear whether or not these are satellites that broke loose during size classification. The $+53\text{, }-63\text{ }\mu\text{m}$ size fraction (Fig. 5c)

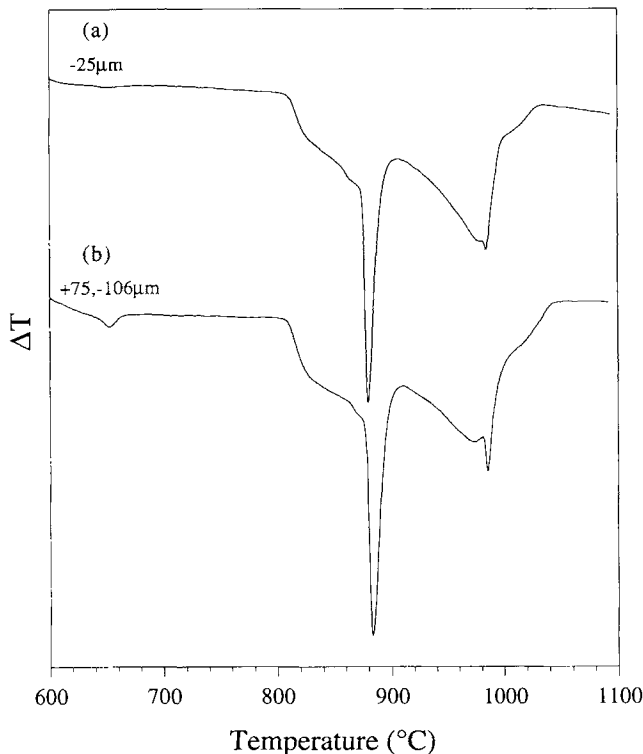


Fig. 4 DTA thermograms obtained while heating (a) $-25\text{ }\mu\text{m}$, and (b) $+75\text{, }-106\text{ }\mu\text{m}$ as-atomized starting powders

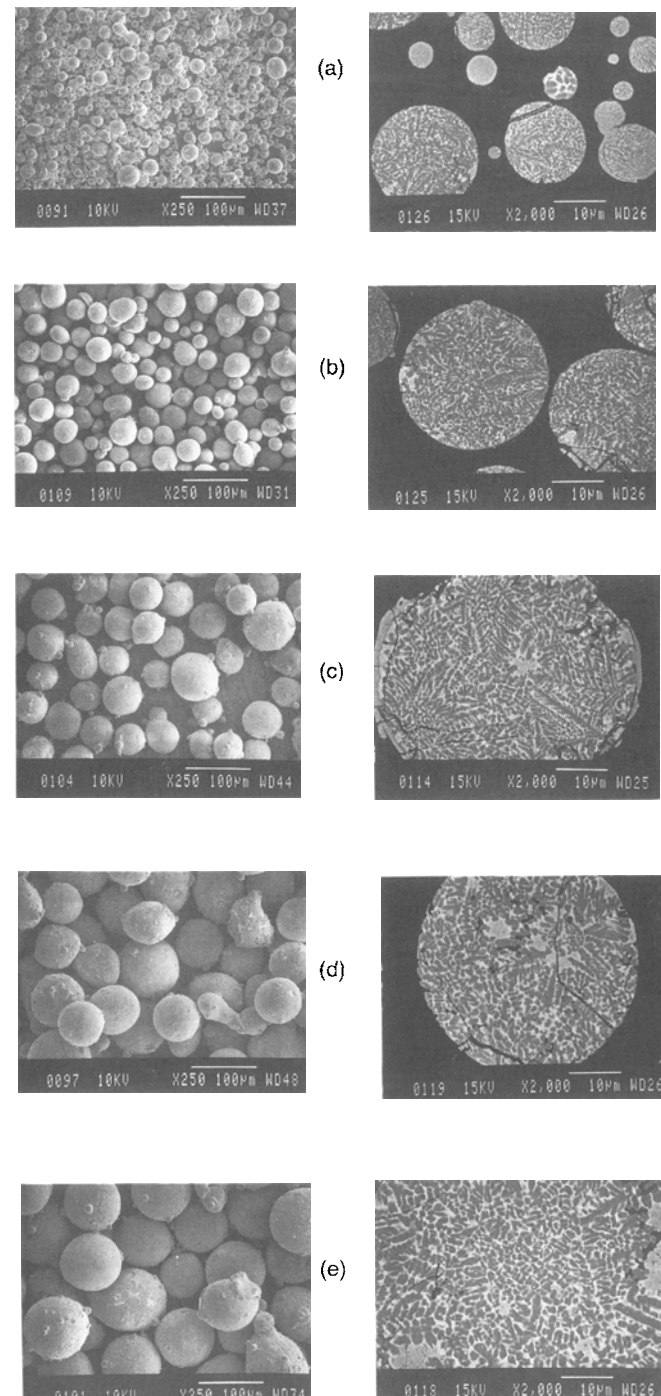


Fig. 5 SEM micrographs of as-atomized starting particles. Images are powder morphologies and polished cross sections of the following particle size fractions: (a) $-25\text{ }\mu\text{m}$; (b) $+25\text{, }-45\text{ }\mu\text{m}$, (c) $+53\text{, }-63\text{ }\mu\text{m}$; (d) $+45\text{, }-75\text{ }\mu\text{m}$; and (e) $+75\text{, }-106\text{ }\mu\text{m}$.

actually appears to be a bimodal distribution; the smaller particles again may have originated from satellites. The polished cross sections illustrate the mixed-phase structure of the atomized particle. The coarser particles tend to show a slightly dendritic structure, while the cellular growth is more dominant in smaller particles.

3.2 Composition and Structure of PS Coatings

The chemical analysis results from coatings removed from hot Cu substrates and thin steel strips are listed in Table 4. The $-25\text{ }\mu\text{m}$ starting powder lost considerable Al during spraying (coatings 1MH, 1MC, 1SH, 1SC, 1*MH, 1*MC, 1*SH, and 1*SC). The $+25\text{,}-45\text{ }\mu\text{m}$ size fraction powder exhibited similar mass loss during spraying, but to a lesser extent. Also, comparison of compositions (e.g., lower Al contents) of coatings sprayed with Mach I and subsonic gun arrangements suggests that the latter configuration and corresponding operating parameters (Table 1) produced a more aggressive environment. This observation is more easily seen with smaller powder size

fraction coatings (e.g., 1SC, 2SC, and 3SC vs 1MC, 2MC, and 3MC, respectively).

Oxygen contents of as-sprayed coatings (Table 4) also varied as a function of the starting powder particle size. Higher O values were measured from the finer powder fractions. In addition, coatings sprayed with the subsonic gun configuration picked up more O than the coatings sprayed with the Mach I configuration; similar behavior between the two spraying conditions was also observed with the annealed starting powder. During spraying, the annealed starting powders gained slightly more O than the as-atomized powders. For a given powder particle size and gun configuration, coatings deposited onto the hot Cu substrates gained more O than the comparable coatings deposited onto the cool steel substrates.

Figures 6 and 7 display XRD patterns obtained from coatings deposited onto hot Cu and cool steel substrates using Mach I and subsonic plasma gun configurations, respectively. Each figure shows the differences in coating structure as a result of substrate temperature; i.e., hot Cu and cool steel substrates. Generally, a hot substrate appears to promote the formation of the ψ phase.

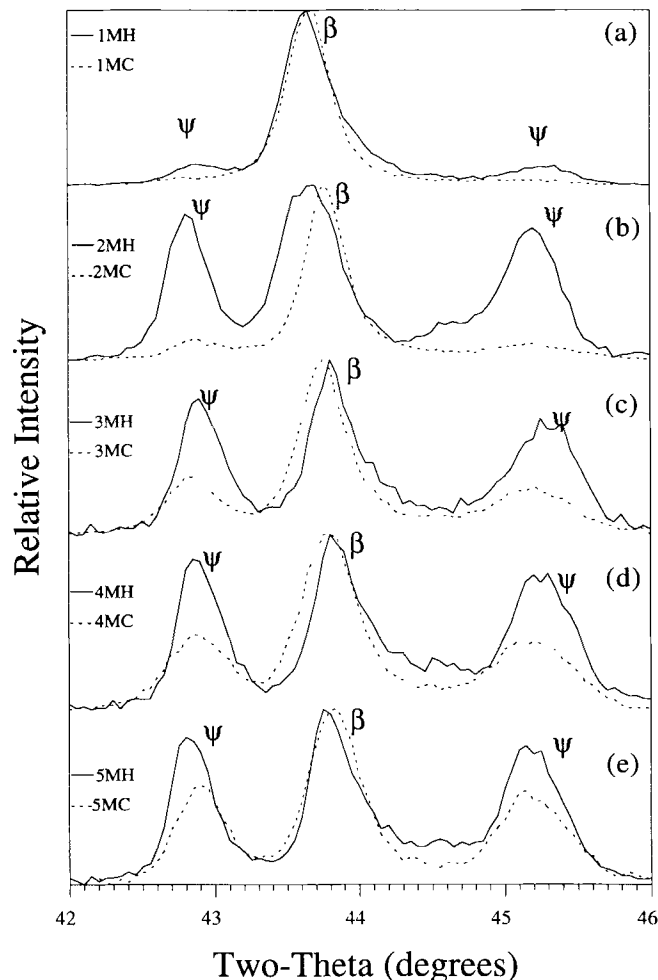


Fig. 6 XRD patterns of PS coatings deposited onto hot Cu and cool steel substrates using a Mach I gun configuration and the following starting powder particle sizes: (a) $-25\text{ }\mu\text{m}$; (b) $+25\text{,}-45\text{ }\mu\text{m}$; (c) $+53\text{,}-63\text{ }\mu\text{m}$; (d) $+45\text{,}-75\text{ }\mu\text{m}$; and (e) $+75\text{,}-106\text{ }\mu\text{m}$. Refer to coating labels and Table 2 to distinguish between different substrates.

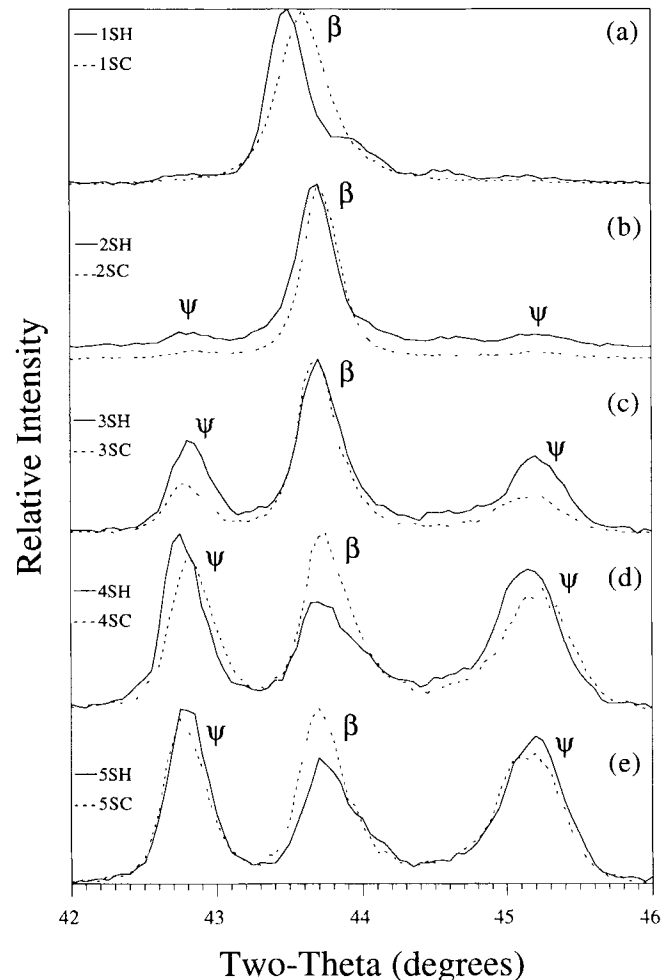


Fig. 7 XRD patterns of PS coatings deposited onto hot Cu and cool steel substrates using a subsonic gun configuration and the following starting powder particle sizes: (a) $-25\text{ }\mu\text{m}$; (b) $+25\text{,}-45\text{ }\mu\text{m}$; (c) $+53\text{,}-63\text{ }\mu\text{m}$; (d) $+45\text{,}-75\text{ }\mu\text{m}$; and (e) $+75\text{,}-106\text{ }\mu\text{m}$. Refer to coating labels and Table 2 to distinguish between different substrates.

Comparison of Fig. 6 and 7 shows that the coatings that were sprayed using the Mach I gun configuration and smaller starting particle sizes (e.g., powder sizes 1, 2, and 3) developed more of the ψ phase. The phase contents of the coatings formed with annealed starting powders (Fig. 8 and 9) are similar to the coatings prepared with the as-atomized powders.

Coatings deposited onto hot Cu substrates are not structurally uniform throughout their thickness. Figures 10 and 11 illustrate the variations in ψ and β contents of as-sprayed coating surfaces and powdered coatings. Analysis of a powdered coating by XRD represents an average phase assemblage throughout the thickness of the coating. In contrast, XRD of an as-sprayed coating surface examines only a few microns of deposited coating. In this study, coating thickness ranged from around 300 μm to near 700 μm ; coarser powder particle sizes produced thicker coatings. The differences between the XRD patterns obtained from as-sprayed surfaces and powdered coatings illustrate the variation of phases throughout the bulk of the coatings. Identical analyses of as-sprayed coating surfaces and powdered coatings were performed on coatings deposited onto cool steel substrates. Although not shown here, there was no discernible difference

between the XRD patterns obtained from as-sprayed surfaces and powdered coatings deposited onto the cool steel substrates. Coatings formed with annealed starting powders followed the same trend as the coatings formed with as-atomized powders deposited onto the hot Cu and cool steel substrates.

Sections of cool steel substrates coated with the different powder size fractions were vacuum annealed at 700 °C for 2 h. The XRD patterns obtained from as-sprayed surfaces of annealed coatings prepared with as-atomized and annealed starting powders are given in Fig. 12 and 13, respectively. Note that the coatings were not removed from their substrates prior to annealing. The XRD patterns in Fig. 12 and 13 reveal that coatings formed with coarser starting powder particle sizes (e.g., >53 μm) and the Mach I gun configuration develop a nearly single-phase ψ structure during vacuum annealing. Coatings deposited using the subsonic gun configuration, with the exception of coating 5SC, generally do not form a single-phase ψ structure; i.e., the cubic β phase is still present.

While the different starting powder size fractions exhibited comparable melting behavior (Fig. 4), the coatings formed with different powder particle sizes showed contrasting behavior.

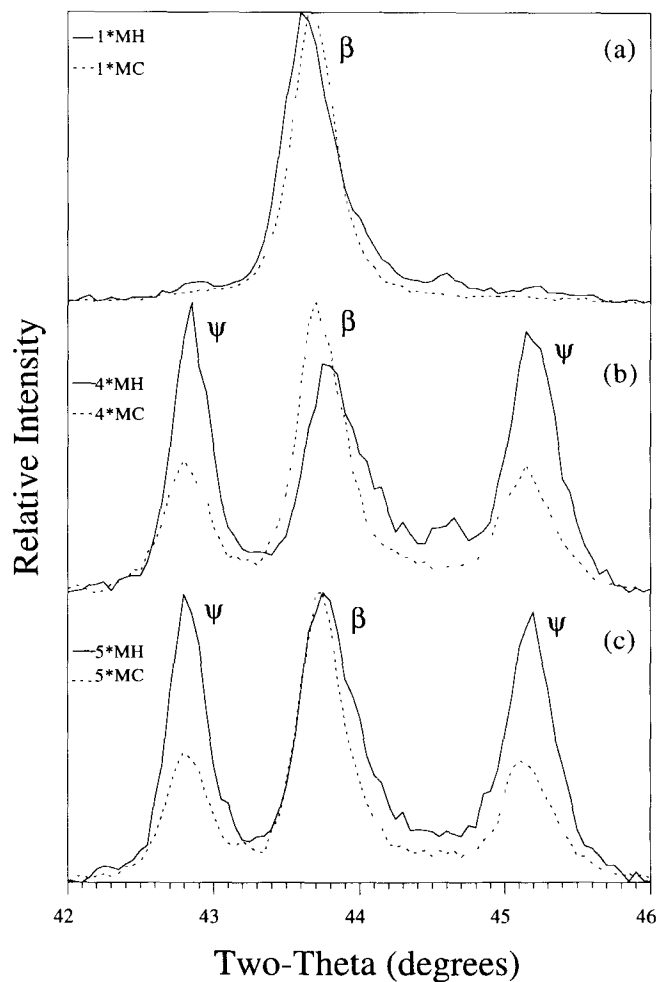


Fig. 8 XRD patterns of PS coatings deposited onto hot Cu and cool steel substrates using a Mach I gun configuration and the following annealed starting powder particle sizes: (a) $-25 \mu\text{m}$; (b) $+45, -75 \mu\text{m}$; and (c) $+75, -106 \mu\text{m}$. Refer to coating labels and Table 2 to distinguish between different substrates.

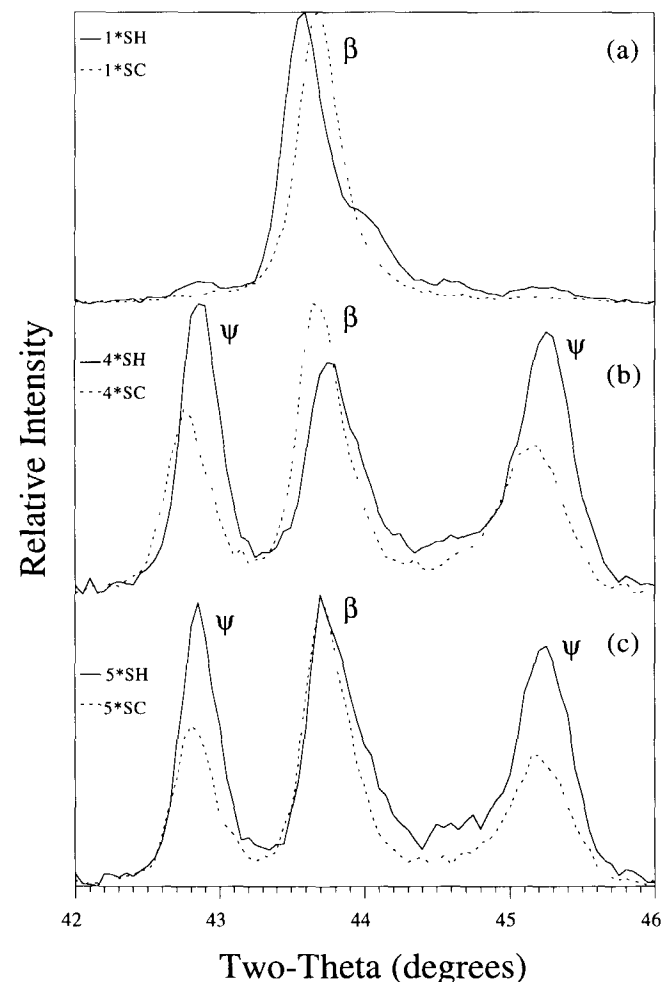


Fig. 9 XRD patterns of PS coatings deposited onto hot Cu and cool steel substrates using a subsonic gun configuration and the following annealed starting powder particle sizes: (a) $-25 \mu\text{m}$; (b) $+45, -75 \mu\text{m}$; and (c) $+75, -106 \mu\text{m}$. Refer to coating labels and Table 2 to distinguish between different substrates.

Table 4 Chemical composition and ψ phase content of PS coatings

Coating label	Composition, wt %				
	Al	Cu	Fe	O	ψ (a)
1MH	35.9	40.9	17.1	2.21	24
2MH	39.0	41.3	16.2	1.15	71
3MH	40.9	39.9	16.3	0.738	70
4MH	41.6	40.2	16.0	0.552	69
5MH	41.7	40.5	16.3	0.456	69
1MC	36.1	42.0	18.6	1.74	10
2MC	40.0	40.7	16.9	0.557	15
3MC	40.7	39.9	16.9	0.294	37
4MC	41.5	39.9	16.9	0.154	43
5MC	40.9	39.7	16.9	0.145	50
1SH	31.3	44.1	19.2	2.43	7
2SH	37.3	41.7	17.4	1.49	20
3SH	38.6	39.8	16.1	0.912	54
4SH	41.3	40.2	16.2	0.594	77
5SH	41.7	39.8	16.2	0.447	79
1SC	29.6	42.8	21.0	2.04	2
2SC	35.3	42.3	18.7	0.971	4
3SC	39.6	40.4	17.1	0.604	28
4SC	40.7	40.1	16.8	0.267	59
5SC	41.0	40.0	16.6	0.231	61
1*MH	31.7	44.4	17.9	...	12
4*MH	41.3	40.4	16.4	0.529	...
5*MH	40.9	40.5	16.3	0.657	71
1*MC	33.3	42.3	19.0	2.08	3
4*MC	40.6	39.7	16.3	0.242	43
5*MC	40.5	39.4	16.3	0.242	42
1*SH	28.0	45.0	20.2	...	4
4*SH	39.4	41.1	16.6	0.764	...
5*SH	39.2	41.9	16.1	0.998	70
1*SC	30.3	42.9	20.5	2.24	2
4*SC	40.0	40.0	16.7	0.332	52
5*SC	40.1	39.7	16.4	0.303	48

Note: Composition of $\text{Al}_{63}\text{Cu}_{25}\text{Fe}_{12}$ is approximately 42.3 wt% Al, 40.0 wt% Cu, and 17.3 wt% Fe (a) ψ phase from powdered coatings is based on calibration curve in Fig. 2.

Table 5 Indentation hardnesses of PS coatings

Coating label	Indentation hardness, $\text{HV}_{0.03}$
1MH	1136 \pm 337
1MC	704 \pm 106
1SH	724 \pm 186
1SC	675 \pm 93
3MH	1039 \pm 257
3MC	981 \pm 134
3SH	909 \pm 87
3SC	745 \pm 94
5MH	859 \pm 112
5MC	846 \pm 178
5SH	890 \pm 87
5SC	879 \pm 157

Figure 14 shows DTA traces obtained from coatings 1SC and 4SC. The finer powder coating, 1SC, does not show a thermal event associated with the ψ phase; i.e., an endothermic peak just below 900 °C. The coarser powder coating, 4SC, on the other hand, shows similar melting behavior to the +45, -75 μm starting powder. Very similar DTA results were obtained with coatings sprayed using the Mach I gun configuration as well as with

annealed starting powders. In general, coatings that lost more Al during spraying produced DTA traces similar to Fig. 14(a).

Variations in coating grain structures paralleled the chemical and structural differences discussed. Coatings deposited onto the hot Cu substrates are denser and show less intergranular cracking than their counterparts sprayed onto cool steel substrates. Figure 15 displays polished cross sections of coatings sprayed with the Mach I plasma gun configuration onto hot and cool substrates. The dense layer at the coating substrate interface on the hot Cu substrates is an oxide layer that formed while pre-heating the Cu substrate. Coating density also varies with starting powder size. Regardless of the substrate temperature, coatings prepared with coarser particles are more porous. Coatings deposited with the subsonic plasma gun configuration exhibit very similar microstructures to the coatings shown in Fig. 15. Annealing the starting powder did not produce any noticeable differences in the grain structure of the coatings.

Indentation hardness measurements from selected coating samples are displayed in Table 5; average values are shown \pm one standard deviation. Coating hardness appears to increase with higher coating density and higher ψ phase content; however, higher hardness values on coatings formed with -25 μm powders may also be due to the presence of oxides within the coating microstructure.

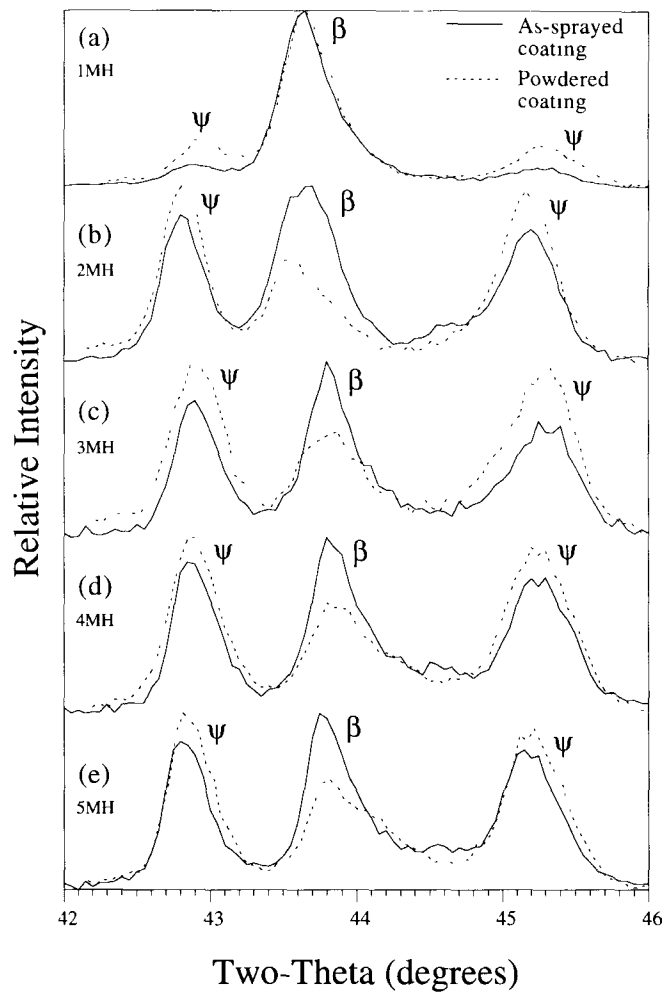


Fig. 10 XRD patterns of as-sprayed and powdered PS coatings deposited onto hot Cu substrates using the Mach I gun configuration and the following starting powder particle sizes: (a) $-25 \mu\text{m}$; (b) $+25, -45 \mu\text{m}$; (c) $+53, -63 \mu\text{m}$; (d) $+45, -75 \mu\text{m}$; and (e) $+75, -106 \mu\text{m}$

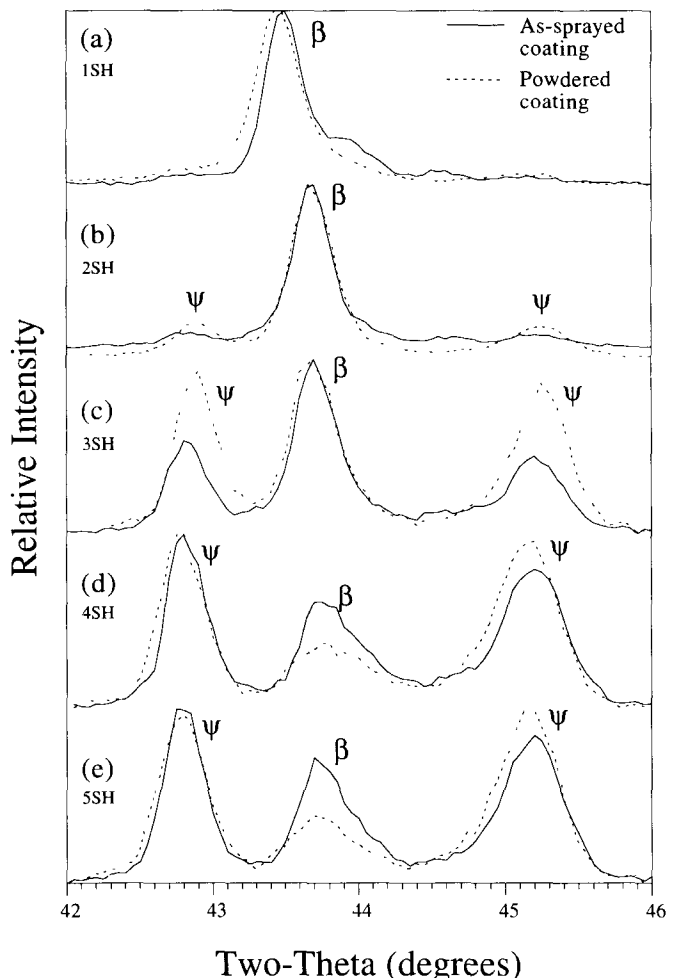


Fig. 11 XRD patterns of as-sprayed and powdered PS coatings deposited onto hot Cu substrates using the subsonic gun configuration and the following starting powder particle sizes: (a) $-25 \mu\text{m}$; (b) $+25, -45 \mu\text{m}$; (c) $+53, -63 \mu\text{m}$; (d) $+45, -75 \mu\text{m}$; and (e) $+75, -106 \mu\text{m}$

4. Discussion

4.1 Starting Powder and Coating Chemistry

4.1.1 Starting Powder

Table 3 shows that the Al, Cu, and Fe contents of the atomized powders do not vary as a function of particle size. Oxygen levels of the atomized powders are higher in the finer, larger surface area powders. As discussed, this strongly suggests that oxygen contamination is present as a surface film rather than as a bulk constituent. Also, results from the XRD (Fig. 3) and DTA (Fig. 4) analyses show the fairly uniform phase structure of the different powder particle size fractions. The coarser starting powder particles have slightly more of the β phase, as shown in Fig. 3(e) and Table 3. Considering the uniformity of the starting powders, the chemistry changes measured in the as-sprayed coatings (Table 4) clearly occurred during spraying.

4.1.2 Coatings

All the coatings appear to have lost some Al during spraying; however, coatings formed with finer powders show a substantial loss of Al. This is consistent with both plasma gun configurations and both starting powders. The coatings that lost the most Al also gained the most oxygen. The annealed starting powders tended to gain more oxygen and lose more Al during spraying than the as-atomized starting powders. Assuming that similar size powders are all molten during spraying, the contrasting starting phase structures of the chemically similar as-atomized and annealed starting powders should not affect the phase structure of the coatings. The chemical variations seen in the coatings formed with as-atomized and annealed powders are, therefore, likely due to initial reactions between the particles and the plasma. For example, if the thermal conductivities of the ψ and β phases are different, then the thermal behavior of multiphase as-atomized and single-phase annealed powders could be different during spraying. The similar compositions of as-sprayed coatings deposited onto hot Cu and cool steel substrates show

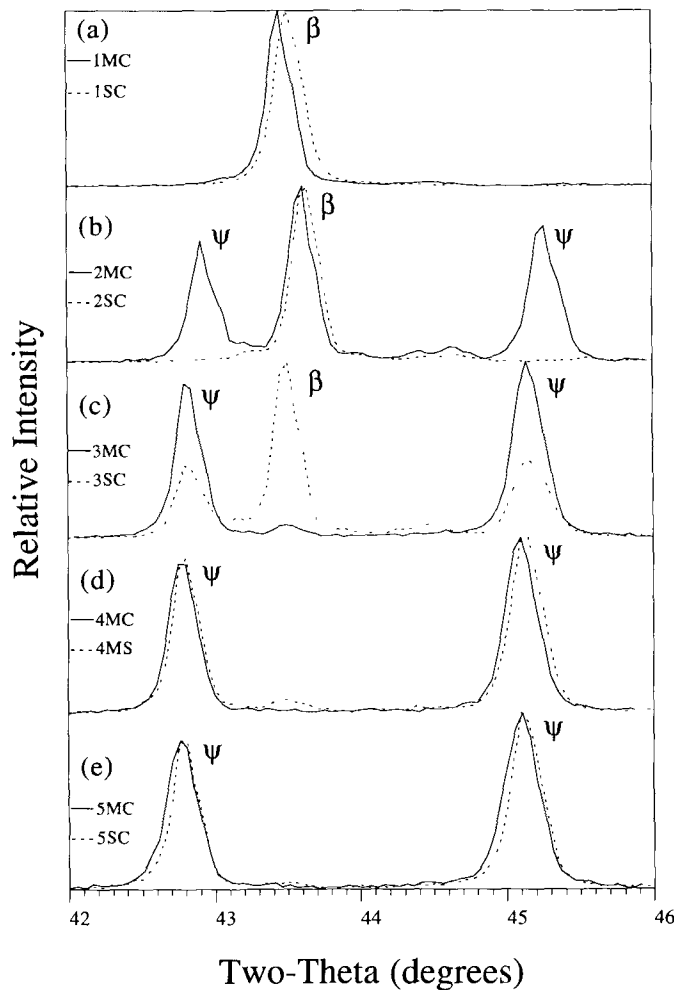


Fig. 12 XRD patterns of vacuum annealed (700 °C) coatings deposited onto cool steel substrates using the following starting powder particle sizes: (a) -25 µm; (b) +25, -45 µm; (c) +53, -63 µm; (d) +45, -75 µm; and (e) +75, -106 µm. Refer to figure legend and Table 2 to distinguish between different gun configurations.

that substrate temperature does not influence final coating chemistry. Therefore, the variation between starting powder and coating composition (e.g., loss of Al) must be occurring prior to deposition onto the substrate.

While the oxygen incorporated into the coating during spraying is likely in the form of Al₂O₃ (Ref 11), the level of oxygen measured by IGF does not account for the total loss of Al. Also, the dissolution technique used to prepare samples for ICP-AES analysis did not leave any residual solid (e.g., Al₂O₃); therefore, Al present as an oxide should be part of the reported values in Table 4. Given this consideration, it appears that Al is lost by vaporization during spraying. If sufficient thermal energy is present to volatilize a portion of the Al₆₃Cu₂₅Fe₁₂ powders, Al should be the most susceptible to vaporization. The vapor pressure of pure Al at temperatures between 1000 and 2000 °C is much higher than the vapor pressure of Cu or Fe (Ref 27). However, the preceding statement presumes that Al, Cu, and Fe are in elemental form. The Al₆₃Cu₂₅Fe₁₂ gas atomized powders are mixtures of intermetallic phases. They would, therefore, be expected to form a ternary solution upon melting during plasma

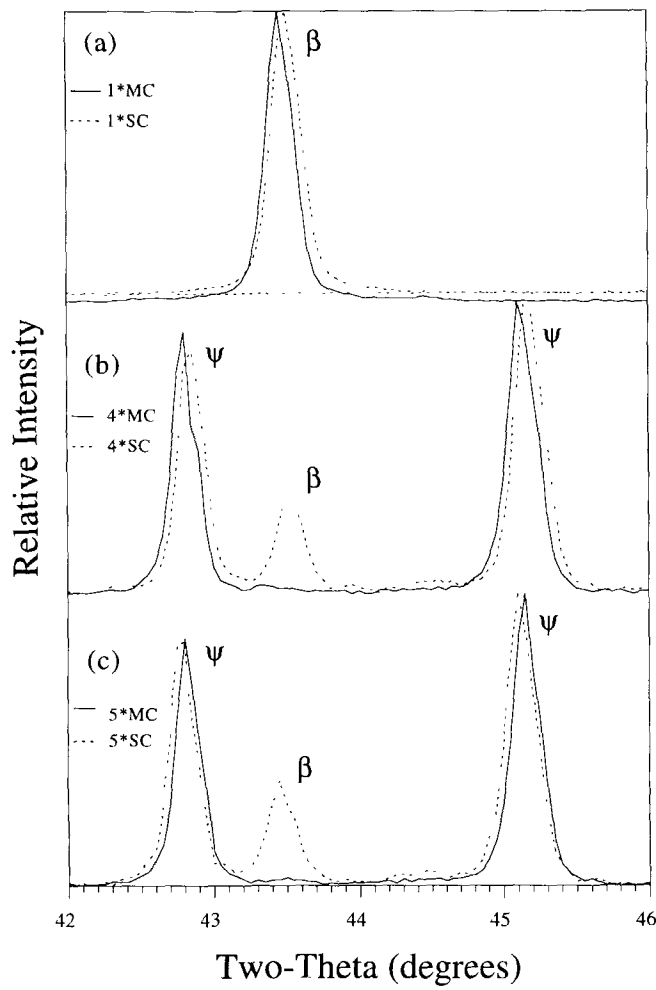


Fig. 13 XRD patterns of vacuum annealed (700 °C) coatings deposited onto cool steel substrates using the following annealed starting powder particle sizes: (a) -25 µm; (b) +45, -75 µm; and (c) +75, -106 µm. Refer to figure legend and Table 2 to distinguish between different gun configurations.

spraying. Depending upon the behavior of the ternary solution (i.e., deviation from ideality) at a given temperature and liquid composition, Al may or may not exhibit a higher partial vapor pressure than Cu or Fe. Deviations from ideality generally decrease as the temperature of the solution increases, so at higher temperatures (e.g., operative temperatures within the plasma), Al would be more likely to have a higher partial vapor pressure than Cu or Fe. Mathematical or experimental analyses of this behavior are well beyond the scope of this current study, particularly in light of the complex melting behavior of the Al-Cu-Fe system and the unknown particle temperature during spraying. Nevertheless, the data in Table 4 show that more Al is lost during spraying than Cu or Fe.

The reasons for the increased loss of Al in the coatings sprayed with the subsonic plasma gun configuration are unclear. The power consumed by subsonic spraying was around 18 kW, while Mach I spraying consumed around 27 kW. However, plasma gas composition and velocity need to be considered as well to predict plasma-powder interactions. Qualitatively, the subsonic parameters provide either more thermal energy to the

powders, which increases Al vaporization, or less kinetic energy, which extends the time for vaporization before solidification.

Selective elemental loss during spraying of alloy powders is common. Perhaps the most well-known case is the decarburization of WC powders during air plasma spraying (Ref 22, 23). Similar reactions leading to mass loss were observed in spraying other refractory metal carbides (Ref 28). Since the reaction products in these examples include volatile species, the material loss is straightforward. Selective vaporization of elements that exist as condensed phases under normal conditions was also observed. For example, air plasma spraying of $\text{YBa}_2\text{Cu}_3\text{O}_{7-\delta}$ superconductor powders resulted in the loss of Cu (Ref 24). Furthermore, recent results showed that fine $\text{Al}_{63}\text{Cu}_{25}\text{Fe}_{12}$ powders (e.g., +5, -25 μm) also lost Al during low-pressure plasma spraying within an argon atmosphere at 200 torr (Ref 29). On the other hand, studies of PS of Al-based intermetallics (e.g., Ni_3Al - NiAl in a low-pressure system) did not provide any detectable loss of Al (Ref 30).

The difference in the tendency for selective elemental loss during PS of Al-Cu-Fe quasicrystal and $\text{YBa}_2\text{Cu}_3\text{O}_{7-\delta}$ powders compared to that for Ni_3Al - NiAl powders is likely due to the lower melting temperatures and lower thermal conductivities of the former systems. Typical thermal conductivities (in $\text{W}/\text{cm} \cdot \text{K}$) reported in the literature for $\text{Al}_{63}\text{Cu}_{25}\text{Fe}_{12}$, $\text{YBa}_2\text{Cu}_3\text{O}_{7-\delta}$, and NiAl are 4 (Ref 31), 10 (Ref 32), and 75 (Ref 33), respectively. Two-phase, i.e., liquid and solid, heat conduction in a spherical particle is seen from the following energy balance equations:

$$\rho_s C_s \frac{\partial T_s}{\partial t} = \frac{1}{r^2} \frac{\partial}{\partial r} \left(r^2 k_s \frac{\partial T_s}{\partial r} \right) 0 \leq r < r_f(t) \quad (\text{Eq 1})$$

$$\rho_l C_l \frac{\partial T_l}{\partial t} = \frac{1}{r^2} \frac{\partial}{\partial r} \left(r^2 d_l \frac{\partial T_l}{\partial r} \right) r_f(t) \leq r \leq r_p \quad (\text{Eq 2})$$

In Eq 1 and 2, ρ is particle density, C is specific heat, T is temperature, k is thermal conductivity, r_p is particle radius, and $r_f(t)$ is the radius of the dynamic solid-liquid boundary. Subscripts s and l refer to solid and liquid states, respectively. The energy balance helps to illustrate how a lower thermal conductivity would require additional time for a particle to become fully molten. This may lead to increased surface liquid temperatures, which would further enhance vaporization. Alloy powders with elemental constituents that have contrasting vapor pressures will therefore be particularly susceptible to selective elemental loss.

Modeling studies were performed to simulate the melting of various size spherical Fe particles within a radio frequency plasma at atmospheric pressure (Ref 34). They predict that smaller particles will more quickly reach a molten state where the additional heat flux available to the particle is used to supply the heat of vaporization. The model estimates that for an assumed set of plasma conditions, a 20 μm diameter Fe particle would vaporize in 3 ms, while a 60 μm diameter Fe particle would require approximately 60 ms to vaporize. This comparison shows the extreme sensitivity of particle size to heat conduction and potential vaporization. These observations agree with the results of the current study and imply that small, lower ther-

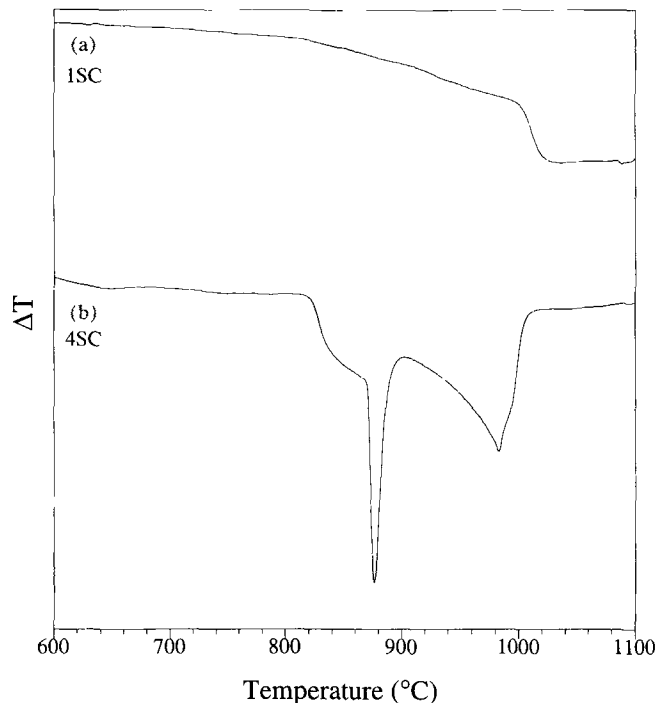


Fig. 14 DTA thermograms obtained while heating coatings deposited onto cool steel substrates using a subsonic gun configuration and the following starting powder particle sizes: (a) -25 μm ; and (b) +45, -75 μm

mal conductivity powders are more sensitive to mass loss through vaporization.

4.2 Coating Structure

4.2.1 Phase Content

The shifts in powder chemistry discussed have a direct impact on the phase structure of the deposited coatings. The substantial loss of Al while spraying the -25 μm powder produced coatings that were all nearly single-phase β as determined by XRD (Fig. 6-9). Coatings prepared with +25, -45 μm powder using the subsonic arrangement also consist mainly of the β phase (Fig. 7b). Coatings prepared with larger starting powder particle sizes lost less Al and formed coatings that contain ψ and β phases (Fig. 6-9). The volume of the ψ phase increases with increasing starting powder particle size (Table 4).

The phases formed during coating are affected not only by compositional changes, as discussed, but also by substrate temperature effects. Coatings sprayed onto hot Cu substrates developed more of the ψ phase than their counterparts deposited onto cool steel substrates (Table 4 and Fig. 6-9). The increased formation of the ψ phase on the hot Cu substrates is likely due to annealing of the solidified coating during deposition. Since the ψ phase is stable at slightly above the estimated substrate surface temperatures (Ref 5), some phase homogenization during annealing may have occurred concurrently with spraying. The driving force would come from the heat provided by the Cu substrate together with the heat of impacting molten droplets. This latter contribution would be more pronounced with the hot Cu substrates than with the cool steel substrates because the higher

temperature reduces the thermal gradient between the impacting droplets and the Cu substrate or, as coating progresses, the freshly deposited coating surface. This could also provide additional time for annealing to occur in the presence of liquid, which would enhance diffusion and phase homogenization.

The temperature of the coating surface appears to decrease with each sequential coating layer deposited onto the hot Cu substrates. This is seen by comparing the XRD patterns obtained from as-sprayed surfaces and from powdered coatings. The as-sprayed coating surfaces represent a coating deposited onto a relatively cooler surface since x-ray penetration is only approximately 5 to 10 μm . The powdered coating represents an integrated series of coating surface temperatures, which would have a higher average substrate temperature than the final as-sprayed surface. Figures 10 and 11 show the higher ψ phase content of the powdered coating samples. The decreasing surface temperature of the coating during spraying effectively reduces the amount of annealing that can occur. The Mach I and subsonic coatings sprayed with the annealed starting powders onto hot Cu substrates exhibited the same behavior as the coatings sprayed with as-atomized starting powders shown in Fig. 10 and 11. The XRD patterns obtained from as-sprayed surfaces and powdered samples of coating deposited on cool steel substrates, however, did not show any differences in ψ or β phase contents. Since the steel substrates were cooled during spraying, no annealing should have occurred, and the as-sprayed surface will be more similar to the bulk of the coating.

The roles of chemistry and solidification behavior on coating structure can be further understood by evaluating the XRD data obtained from coatings deposited onto cool steel substrates that were subsequently vacuum annealed. For example, vacuum annealing of the 1MC and 1SC coatings did not change their structure (Fig. 12a). The 2SC coating did not change its structure during annealing, but the 2MC coating showed an increase in ψ phase (Fig. 12b). This latter change is more evident if the 2MC curve in Fig. 12b is compared to the XRD trace from the as-sprayed 2MC coating shown in Fig. 6(b). Further increases in starting powder particle size resulted in coatings that formed higher ψ content coatings during vacuum annealing (Fig. 12c-e). The Mach I coatings sprayed with coarser particles (3MC, 4MC, and 5MC) all developed a nearly single-phase ψ structure during annealing. The corresponding subsonic coatings followed the same trend, but the 3SC and 4SC coatings still had some β phase present. The Mach I coatings formed with annealed starting powders behaved similarly, as shown in Fig. 13. Coarser annealed powders sprayed with subsonic conditions (4*SC and 5*SC), however, still showed some residual β phase after annealing (Fig. 13b and c).

The above XRD results correlate very well with ICP-AES chemical analyses (Table 4). Powders that lose the most Al during spraying exhibit higher concentrations of the β phase in both as-sprayed and vacuum annealed conditions. The coatings that were measured to contain no more than 40 wt% Al follow this behavior. However, note that this value represents an average composition. Localized chemical inhomogeneities that control the observed change in phase distribution likely exist. Figure 14 shows further evidence of phase differences between coatings deposited with finer (1SC) particles and coarser (4SC) particles. The 4SC coating clearly shows melting of the ψ phase below

900 °C, followed by final melting of β and λ phases. The 1SC coating only shows one endothermic reaction around 1000 °C, which likely corresponds to melting of the β phase.

The final chemistry of the coatings that were low in Al could have shifted out of the ψ single-phase region of the Al-Cu-Fe phase diagram. For example, the composition of the 2MC coating is approximately $\text{Al}_{61}\text{Cu}_{26}\text{Fe}_{12}$ (Table 4). According to a proposed isothermal section at 700 °C (Ref 5), the composition of the 1SC coating moved out of the single-phase ψ region into a ψ -rich portion of the two-phase region containing the β and ψ phases. Since $\text{Al}_{61}\text{Cu}_{26}\text{Fe}_{12}$ is a bulk value, there are likely localized compositional gradients throughout the coating that contribute to the XRD pattern obtained from coating 2MC shown in Fig. 6(b). Nevertheless, the chemistry and structure data clearly indicate that selective elemental loss during PS will affect the resulting phase assemblage of the coating.

Results show that the phases developed in coatings sprayed with $\text{Al}_{63}\text{Cu}_{25}\text{Fe}_{12}$ powders depend upon both final chemistry and substrate temperature effects. Although most as-deposited coatings contain ψ and β phases, as long as they did not lose too much Al (e.g., ~3 wt%) during spraying, the coatings may still be vacuum annealed to form a nearly single-phase ψ structure. However, regardless of the substrate thermal history, if the coating loses enough Al during spraying, it will not form the quasi-crystalline ψ phase during subsequent vacuum annealing. Absolute conclusions are difficult to reach regarding phase equilibrium of the Al-Cu-Fe system with plasma sprayed coatings because of the unknown solidification path. Surface oxidation could cause localized chemistry shifts if Al is further consumed to form an oxide. This effect was seen during oxidation of Al-Cu-Fe powders and bulk coatings (Ref 13).

4.2.2 Microstructure

Starting powder particle size and substrate temperature affect the grain structure of the PS coatings. Figure 15 shows scanning electron microscope (SEM) micrographs from polished cross sections of the Mach I coatings deposited onto hot and cool substrates. These coatings were sprayed with as-atomized powder. The subsonic coatings and the coatings formed with annealed starting powders were very similar to the coatings presented in Fig. 15. The coatings sprayed onto hot Cu substrates are significantly less porous than those sprayed onto cool steel substrates. Particles contacting the hotter surface should exhibit increased deformation and liquid flow. In addition to variations in grain structure due to substrate temperature, Fig. 15 also reveals the impact of starting powder particle size. The 1MH and 1MC coatings are denser than the coatings prepared with coarser powder particles. However, oxides are visible along the splat boundaries of the 1MH and 1MC coatings. The presence of oxides is expected given the oxygen gained during spraying of the finer powder particles (Table 4). Coarser starting powder particles lead to increased levels of porosity and intergranular cracking. The coatings sprayed with the coarser size fractions also contain unmelted particles. These are seen as areas with features similar to the solidified structure of the gas atomized powders (Fig. 5).

Variations in the as-sprayed coating microstructures produced different indentation hardness values. Data obtained from coatings prepared with a range of starting powder particle sizes

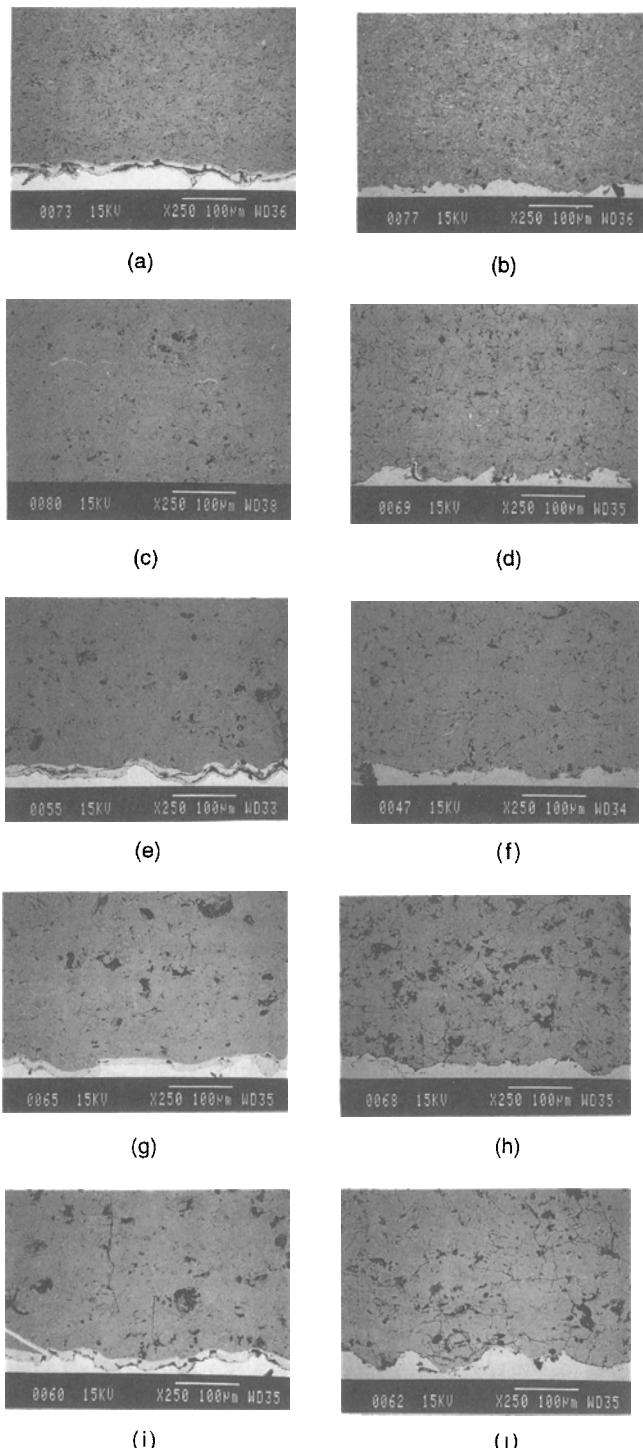


Fig. 15 SEM micrographs of coatings formed with a Mach I gun configuration on hot Cu substrates (left-hand column) and cool steel substrates (right-hand column) using the following starting powder particle sizes: (a) and (b) -25 µm; (c) and (d) +25, -45 µm; (e) and (f) +53, -63 µm; (g) and (h) +45, -75 µm; and (i) and (j) +75, -106 µm

are given in Table 5. The higher density and oxides present in the 1MH, 1MC, 1SH, and 1SC coatings contribute to a higher hardness. Hardness values of coatings sprayed onto hot Cu substrates are higher than those of coatings formed on cool steel substrates. This is due to a combination of lower porosity and a higher fraction of the ψ phase in these coatings. The β phase was

reported to be softer than the ψ phase within the Al-Cu-Fe system (Ref 8). Hardness measurements were not made with annealed powder coatings.

5. Conclusions

Starting powder particle size is a universally important variable in thermal spraying processes. It is particularly critical in PS of Al₆₃Cu₂₅Fe₁₂ quasi-crystalline powders. The low thermal conductivity of the quasicrystalline ψ phase provides greater opportunity to overheat and partially vaporize powders during spraying. Finer particles (e.g., -25 µm) exhibited substantial vaporization of Al during PS with Mach I and subsonic gun configurations. This material loss shifted the coating composition away from the single-phase ψ region of the Al-Cu-Fe phase diagram. Coatings that lost more than several atomic percent Al were mostly single-phase β and did not change structure during vacuum annealing at 700 °C. Coatings that lost less Al consisted of ψ and β phases in varying amounts depending on starting powder particle size and substrate temperature. These coatings could be annealed in vacuum at 700 °C to form a nearly single-phase ψ structure.

The phases formed in the coatings were not only affected by chemistry shifts during spraying, but also by substrate temperatures. The heat provided by the hot Cu substrates appears to partially anneal the deposited coating during spraying. Coatings deposited onto hot substrates were more dense, harder, and richer in the ψ phase than coatings deposited onto cool substrates.

This study shows how critical it is to control powder particle size during PS of Al₆₃Cu₂₅Fe₁₂ powders. Results also suggest that it is possible to further refine PS parameters to produce denser coatings with higher ψ phase contents. Studies are in progress to further understand the role of other PS conditions on Al₆₃Cu₂₅Fe₁₂ coating microstructure.

Acknowledgments

The authors thank R. Hofer and C. Bradley for their expertise in performing the chemical analyses. This study was performed at Ames Laboratory, Iowa State University, and was supported by the Director of Energy Research, Office of Basic Energy Sciences, United States Department of Energy under contract No. W-7405-ENG-82 and by the State of Iowa for the Iowa State University Institute for Physical Research and Technology administered by the Center for Advanced Technology Development.

References

1. A.I. Goldman and M. Widom, Quasicrystal Structure and Properties, *Ann. Rev. Phys. Chem.*, Vol 42, 1991, p 685-729
2. D. Shechtman, I. Blech, D. Gratias, and J. W. Cahn, Metallic Phase with Long-Range Orientational Order and No Translational Symmetry, *Phys. Rev. Lett.*, Vol 53 (No. 20), 1984, p 1951-1953
3. C. Janot, J. M. Dubois, and M. de Boissieu, Quasiperiodic Structures: Another Type of Long-Range Order for Condensed Matter, *Amer. J. of Phys.*, Vol 57, 1991, p 972-987
4. D. Gratias, Y. Calvayrac, J. Devaud-Rzepski, F. Faudot, M. Harmelin, A. Quivy, and P. Bancel, The Phase Diagram and Structures of the Ternary Al-

CuFe System in the Vicinity of the Icosahedral Region, *J. Non-Cryst. Solids*, Vol 153, 154, 1993, p 482-488

5. F.W. Gayle, A.J. Shapiro, F.S. Biancaniello, and W.J. Boettinger, The Al-Cu-Fe Phase Diagram: 0 to 25 At. Pct Fe and 50 to 75 At. Pct Al—Equilibria Involving the Icosahedral Phase, *Metall. Trans. A*, Vol 23, 1992, p 2409-2417
6. J.M. Dubois, A. Proner, B. Bucaille, Ph. Cathonnet, C. Dong, V. Richard, A. Pianelli, Y. Massiani, S. Ait-Yaaza, and E. Belin-Ferre, Quasicrystalline Coatings with Reduced Adhesion for Cookware, *Ann. Chim. Fr.*, Vol 19, 1994, p 3-25
7. J.M. Dubois, S.S. Kang, and J. Von Stebut, Quasicrystalline Low Friction Coatings, *J. Mater. Lett.*, Vol 10, 1991, p 537-541
8. U. Köster, W. Liu, H. Leibertz, and M. Michel, Mechanical Properties of Quasicrystalline and Crystalline Phases in Al-Cu-Fe Alloys, *J. Non-Crystall. Solids*, Vol 153, 154, 1993, p 446-452
9. J.M. Dubois, S.S. Kang, and Y. Massiani, Application of Quasicrystalline Alloys to Surface Coatings of Soft Metals, *J. Non-Crystall. Solids*, Vol 153, 154, 1993, p 443-445
10. E. Hornhogen and M. Schandl, Probing Mechanical Properties of Quasicrystalline Aluminum Alloys, *Z. Metallkd.*, Vol 83, 1992, p 128-131
11. S.L. Chang, W.B. Chin, C.-M. Zhang, C.J. Jenks, and P.A. Thiel, Oxygen Absorption on a Single Grain, Quasicrystal Surface, *Surf. Sci.*, Vol 337, 1995, p 135-146
12. D.J. Sordelet, M.J. Kramer, J.E. Anderson, and M.F. Besser, Microstructural Evolution, Oxidation and Wear of Al-Cu-Fe Quasicrystalline Coatings, *Proc. of the 5th International Conference on Quasicrystals*, C. Janot and R. Mosseri, Ed., World Scientific, 1995, p 778-785
13. S.S. Kang and J.M. Dubois, Influence of the Annealing Atmosphere on the Formation of Al-Cu-Fe Quasicrystals, *J. Mater. Res.*, in press 1996
14. K.F. Kelton, Quasicrystals: Structures and Stability, *Int. Mater. Rev.*, Vol 38, 1993, p 105-136
15. A.P. Tsai, A. Inoue, and T. Masumoto, A Stable Quasicrystal in Al-Cu-Fe, *Jpn. J. Appl. Phys.*, Vol 26, 1987, p L1505-1507
16. S.S. Kang and J.M. Dubois, Compression Testing of Quasicrystalline Materials, *Philos. Mag. A*, Vol 66, 1992, p 151-163
17. J. Shield, M.J. Kramer, and R.W. McCallum, Plastic Deformation in an Al-Cu-Fe Alloy, *J. Mater. Sci.*, Vol 8, 1993, p 1199-1203
18. A.J. Bradley and H.J. Goldschmidt, X-Ray Study of Slowly Cooled Iron-Copper-Aluminum Alloys Part I.—Alloys Rich in Iron and Copper, *J. Inst. Met.*, Vol 65, 1939, p 389-402
19. A.J. Bradley and H.J. Goldschmidt, An X-Ray Study of Slowly Cooled Iron-Copper-Aluminum Alloys Part II.—Alloys Rich in Aluminum, *J. Inst. Met.*, Vol 65, 1939, p 403-418
20. D.J. Sordelet, M.J. Kramer, and O. Unal, Effect of Starting Powders on Controlling Microstructural Development of Al-Cu-Fe Quasicrystalline Plasma Sprayed Coatings, *J. Thermal Spray Tech.*, Vol 4 No. 3, 1995, p 235-244
21. E. Kubel, Jr., Powders Dictate Thermal Spray Coating Properties, *Adv. Mater. Proc.*, Vol 138, 1990, p 24-26
22. D. Tu, S. Chang, C. Chao, and C. Lin, Tungsten Carbide Phase Transformation During the Plasma Spray Process, *J. Vac. Sci. Technol.*, Vol A3, 1985, p 2479-2482
23. M.E. Vinayo, F. Kassobji, J. Guyonnet, and P. Fauchais, Plasma Sprayed WC-Co Coatings: Influence of Spray Conditions (Atmospheric and Low Pressure Plasma Spraying) on the Crystal Structure, Porosity and Hardness, *J. Vac. Sci. Technol.*, Vol A3, 1985, p 2482-2489
24. R.A. Neiser, "Structure-Processing-Property Relationships in Air Plasma Sprayed $YBa_2Cu_3O_{7-\delta}$," Ph.D. thesis, State University of New York at Stony Brook, Department of Materials Science and Engineering, Stony Brook, NY, 1987
25. S. Ebald and F. Spaepen, The Body-Centered-Type Icosahedral Reciprocal Lattice of the Al-Cu-Fe Quasi-Periodic Crystal, *J. Mater. Res.*, Vol 4, 1989, p 39-43
26. D.J. Sordelet and J.E. Shield, Ames Laboratory, Iowa State University, unpublished research 1995
27. *Metals Handbook*, Desk Edition, H.E. Boyer and T.C. Gall, Ed., American Society for Metals, 1985, p 1-54
28. S. Sampath and S.F. Wayne, Plasma Sprayed Mo-Mo₂C Composites. Microstructure and Properties, *Thermal Spray Coatings: Research, Design and Applications*, C.C. Berndt and T.F. Bernecki, Ed., ASM International, 1993, p 397-403
29. D.J. Sordelet, P.D. Krotz, R.L. Daniels, Jr., and M.F. Smith, Microstructure and Wear Behavior of Quasicrystalline Thermal Spray Coatings, *1995 Advances in Thermal Spray Science and Technology*, C.C. Berndt and S. Sampath, Ed., ASM International, 1995, p 627-632
30. R.A. Neiser, private communication, Sandia National Laboratories, NM, 1995
31. J.M. Dubois and P. Weinland, Coating Materials for Metal Alloys and Metals and Method, U.S. Patent 5,204,191, April 1993
32. J.L. Cohn, S.A. Wolf, T.A. Vanderah, V. Slevamanickam, and K. Salama, Lattice Thermal Conductivity of $YBa_2Cu_3O_{7-\delta}$, *Physica C*, Vol 192, 1992, p 435-442
33. R. Darolia, NiAl Alloys for High-Temperature Structural Applications, *JOM*, 1991, p 44-48
34. T. Yosheda and K. Akashi, Particle Heating in a Radio-Frequency Plasma Touch, *J. Appl. Phys.*, Vol 48, 1977, p 2252-2260